A New Ankle Foot Orthosis: Modeling and Control

A. Gmerek*, M. Davoodi*, N. Meskin*, E. S. Tehrani† and R. E. Kearney†
* Department of Electrical Engineering, Qatar University, Doha, Qatar
Emails: gmerek.artur@gmail.com, davoodi.mr@qu.edu.qa, nader.meskin@qu.edu.qa
† Department of Biomedical Engineering, McGill University, Montreal, QC H3A 2B4, Canada.
Emails: ehsan.sobhani@mail.mcgill.ca, robert.kearney@mcgill.ca

***Abstract*—This paper studies the derivation of kinematic and dynamic models of a newly developed active ankle foot orthosis (AFO) that was designated for testing gait-assistive compliance control algorithms. The AFO is characterized with a closed-loop chain structure and powered by a linear ServoTube motor making it very fast and responsive. The paper first derives kinematic and dynamic models for the AFO. Then, a torque controller is developed based on the dynamic model of the AFO and it is shown that the AFO is able to track the position and velocity of the desired trajectory with a satisfactory accuracy.**

I. Introduction

Ankle joint impairments due to joint inflammation, arthritis, sprain, stroke and other neuromuscular diseases are one of the most common reasons for altered gait and problems during walking [1]. Many of these cases can be treated by short-term rehabilitation, surgery, or medication but some require long-term rehabilitation or the use of ankle foot orthoses (AFOs) to provide support during walking. These AFOs can ameliorate the impact of impairments that affect gait, and therefore, improve the quality of life.

Passive AFOs (e.g. rigid or semi-rigid ankle braces) are commonly used to improve gait abnormalities by keeping the ankle joint angle close to 90 degree [2]. However, long-term use of these passive devices is dangerous since they can cause disuse muscle atrophy of muscles and neural degeneration of the neural system [3]. Moreover, they are useful for low-speed walking rather than for normal or fast walking where there is a need for additional energy for propulsion at the plantar flexion phase [4]. Consequently, researchers have been developing semi-active (resistive) and active (assistive) AFOs to help impaired individuals to walk more naturally. Typically these devices incorporate an actuator and control system to modulate the torque generated by a patient [5].

Different kinds of actuators have been used for active AFOs. These actuators typically have low inertia to allow higher mobility due to the wearable nature of the robot. Moreover, they should be inherently backdriveable to ensure the safety of the user [6]. One of the most popular actuators with these characteristics are series elastic actuators (SEA) in which an electric motor is placed in series with a compliant elastic element [7]. Pneumatic [8] and hydraulic [9] actuators have also been used due to their high power to weight ratio and inherent compliance [10]. Conventional electric drives have also been used in some designs [11].

To be useful, an active AFO must have an effective control strategy. Various types of control structures have been described in the literature [4]. In [12], a trajectory tracking, proportional-derivative (PD) controller was described for an active orthosis actuated by a linear motor with a series elasticity element. This controller used an adjustable gait pattern as a reference for the motor position. In [7], a variable-impedance active ankle foot orthosis powered by SEA was described and an adaptive control structure was developed to assist drop-foot gait. In [13], a PID closed-loop control system was chosen for position and speed control of an active orthosis actuated by a DC servo motor. In [14], a bio-inspired soft wearable robotic device powered by pneumatic artificial muscle actuators was designed for ankle foot rehabilitation. An identified linear time-invariant (LTI) model of the AFO was obtained. Then, the controllability of the system was experimentally demonstrated using an LTI controller. In [15], proportional myoelectric control strategy was used for an AFO driven by artificial pneumatic muscles.

The objectives of this paper are to develop model and control system for a new active ankle foot orthosis for the first time in the literature. The contributions of this paper are summarized as follows. First, the kinematic model of the new active AFO, which is necessary to develop the dynamic model of it, is obtained. Second, the dynamic model of the considered AFO is developed by using the Euler-Lagrange equation. Third, based on the AFO inverse dynamics, an inverse dynamics control strategy is proposed. Fourth, the results are validated experimentally.

II. Description of the AFO

The new developed active AFO device has one degree of freedom (DoF) that can only act in the sagittal plane using a ServoTube motor. It includes an artificial leg and the AFO that were printed on the 3D printer from polylactic acid plastic (PLA) and then placed in the metal frame, as presented in Figure 1(a).

The AFO was designed to fit well on a human leg, therefore, it consists of a hollow shank (to be placed on a leg) and a foot part (to be placed on a shoe) as presented in Figure 1(b). The shank part was fixed to a human shank via the ski braces and

This publication was made possible by NPRP grant No. NPRP 6 - 463 - 2 - 189 from the Qatar National Research Fund (a member of Qatar Foundation). The statements made herein are solely the responsibility of the authors.

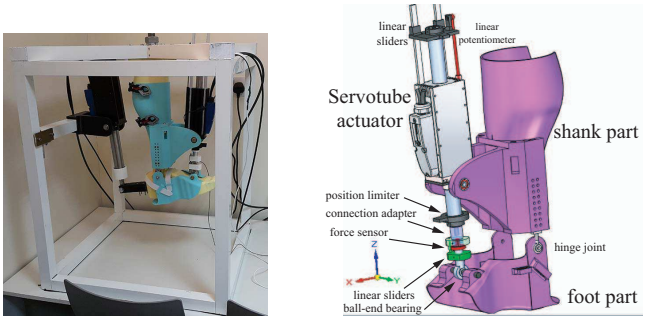

(a) (b)

Fig. 1: The proposed active AFO (a) the real system, (b) the CAD design of the AFO.

the foot part was attached with the velcro stripes as shown in Figure 1(a). The shank and foot parts were connected to each other via the hinged joint and the actuator. The hinge joints, as well as the rod's attachment joint to the foot part of the AFO, consists of spherical ball bearings which are characterized with low friction. This solution allow to compensate nonlinearities, and to control the tilting of a patient. The forcer of the actuator was attached with a trunnion joint to the shank part. This attachment point was optimized so that the AFO would be as compact as possible and would be able to achieve the required range of motion.

The rod's attachment joint (ball-end bearing) was attached to an in-line force sensor, and this sensor was connected to the rod via a mechanical adapter as illustrated in Figure 1(b). The load cell should have been mounted in-line to a load, otherwise the sensor could be damaged. Consequently, in order to assure that forces are only acted inline, the special sliders were designed to permit motion in one axis only. It was also necessary to create linear sliders to lock the rotation of the ServoTube actuator as shown in Figure 1(b).

For the position sensor, the ELPM series linear potentiometer with the maximum stroke of 150 mm was used. This potentiometer has a ruggedised IP67 sealed aluminum housing, a elastomer damped wiper for shock and vibration durability, and self-aligning pivot bearing mountings. For the force sensor, the in-line sensor was used produced by *Futek Advanced sensor technology, INC.*, model - LCM 200. The sensor is able to measure both tension and compression forces. It weighs only 17 g and the natural frequency of the sensor is 26.8 kHz. This sensor is used together with a strain gauge amplifier characterizes with a bandwidth of 10 kHz.

The actuator was considered as a STA2504 Servotube motor produced by DunkerMotoren (the front actuator in Figure 1(a)). This is substantially a linear drive which has wrapped into a tube. It consists of two parts that are moving in relation to each other: a forcer and a rod. This actuator is characterized with high velocity, accuracy, response and backdrivability. As is shown in Figure 1(a), a rear actuator (ServoTube XTA3804 drive) has also been used in the test setup to emulate the human's muscles and also to excite the AFO in the case for identification purposes.

TABLE I: The values of parameters (precise meaning of the symbols are marked in Fig. 2)

symbol	meaning	value
l	The length of a shank part of the orthosis (measured vertically)	300 [mm]
w	Half of the width of the orthosis (on y-level)	40 [mm]
e	The horizontal safety margin	10 [mm]
r_1	The vertical distance between an ankle joint and the shank part	55 [mm]
r_3	The minimum distance between an ankle joint and the actuator's attachment to the foot part	150 [mm]
α_p	The angle of an ankle joint in maximum plantarflexion position	$+41^\circ$
α_d	The angle of an ankle joint in maximum dorsiflexion position	21°
x	The x-coordinate of actuator's attachment point	125 mm
y	The y-coordinate of actuator's attachment point	102 mm
f	The length of actuator's rod	445 mm
α	The angle of an ankle joint	*var*
β	The angle between upper part of the actuator and the horizontal attachment line x	*var*
d	The length of an actuator's rod (segment CB)	*var*

The higher-level AFO's controller is the *Quanser PCI* card which control the *Xenus* controller - an amplifier that directly drive the actuator. The *Xenus* amplifier is programmable and able to drive the motor in position, velocity, or current modes. The *Quanser* card is compatible with *Matlab Real Time Toolbox*, and control the *Xenus* amplifier via analog and digital signals. All sensors were connected to the *Quanser* control card via analog inputs.

As a summary, this device is characterized with high performance in relation to velocity and frequency response, and equipped with a drive which is highly backdrivable. These features makes it ideal to test advanced compliance control algorithms designating for assisting in walking.

III. The kinematic model of the AFO

A kinematic model of the orthosis is needed to map the output of the linear potentiometer (linear position d) to the ankle joint (angular position α), and to develop the dynamic model of the orthosis. Table I defines the parameters, used to derive this model. Figure 2 shows the kinematic structure of the orthosis. The relationship between d and α can be derived based on this figure. By applying the law of Cosines on $\triangle FAB$ and $\triangle FCB$, it follows that:

$$\begin{aligned}(l+r_1)^2 + r_3^2 + 2(l+r_1)r_3\sin(\alpha) = d^2 + \\ x^2 + (l-y)^2 + 2d\sqrt{x^2+(l-y)^2}\cos(\beta-\nu),\end{aligned} \tag{1}$$

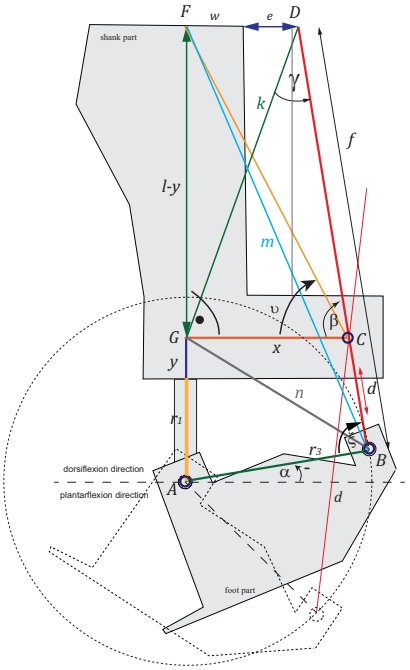

Fig. 2: The geometrical relationship in the AFO.

which gives the relation between the angles α and β. From Figure 2, it can be seen that the angle ν can be expressed as:

$$\nu = \text{arctg}(\frac{l-y}{x}). \tag{2}$$

Consequently, by using the trigonometric subtraction formulas for $\cos(\beta - \nu)$ in (1), it follows that:

$$(l+r_1)^2 + r_3^2 + 2(l+r_1)r_3\sin(\alpha) = d^2 + x^2 + (l-y)^2 + 2d\sqrt{x^2+(l-y)^2}\left(\frac{\cos\beta}{\sqrt{(\frac{l-y}{x})^2+1}} + \frac{(\frac{l-y}{x})\sin\beta}{\sqrt{(\frac{l-y}{x})^2+1}}\right),$$

which can be rewritten as:

$$h^2\sin^2\alpha + [x^2+(l-y)^2]\cos^2\beta + 2gh\sin\alpha - 2gx\cos\beta - 2hx\sin\alpha\cos\beta + g^2 - (l-y)^2 = 0, \tag{3}$$

where

$$g = \frac{(l+r_1)^2 + r_3^2 - d^2 - x^2 - (l-y)^2}{2d}, h = \frac{(l+r_1)r_3}{d}. \tag{4}$$

The angle β is also needed to define the relationship between α and d. Applying the Cosine law to $\triangle GCD$ and $\triangle GAB$, it follows that:

$$k^2 = (f-d)^2 + x^2 - 2x(f-d)\cos(\beta), \tag{5}$$

$$n^2 = (y+r_1)^2 + r_3^2 - 2(y+r_1)r_3\cos(\frac{\pi}{2}+\alpha) = (y+r_1)^2 + r_3^2 + 2(y+r_1)r_3\sin\alpha. \tag{6}$$

while from $\triangle GDB$ and $\triangle GDC$, we have:

$$n^2 = k^2 + f^2 - 2kf\cos(\gamma), \tag{7}$$

$$x^2 = k^2 + (f-d)^2 - 2k(f-d)\cos(\gamma). \tag{8}$$

Setting the right sides of (6) and (7) equal to each other, and substituting $\cos\gamma$ from (8), gives:

$$(f-d)\big[(y+r_1)^2 + r_3^2 + 2(y+r_1)r_3\sin\alpha - fd\big] - fx^2 = -dk^2. \tag{9}$$

Finally, from (5) and (9), it follows that:

$$\cos\beta = \Omega(x,y,d) + \Psi(x,y,d)\sin\alpha, \tag{10}$$

where $\Omega(x,y,d)$ and $\Psi(x,y,d)$ are the auxiliary variables:

$$\Omega(x,y,d) = \frac{1}{2xd}\Big((y+r_1)^2 + r_3^2 - d^2 - x^2\Big), \quad \Psi(x,y,d) = \frac{(y+r_1)r_3}{xd}, \tag{11}$$

which will be abbreviated to Ω and Ψ. Substituting (10) into (3), gives:

$$\Xi(\mathbf{x},\mathbf{y},\mathbf{d})\cdot\sin^2\alpha + \Upsilon(\mathbf{x},\mathbf{y},\mathbf{d})\cdot\sin\alpha + \Gamma(\mathbf{x},\mathbf{y},\mathbf{d}) = 0, \tag{12}$$

where:

$$\Xi(\mathbf{x},\mathbf{y},\mathbf{d}) = h^2 + \Psi^2[x^2+(l-y)^2] - 2hx\Psi,$$
$$\Upsilon(\mathbf{x},\mathbf{y},\mathbf{d}) = 2\big[\Omega\Psi[x^2+(l-y)^2] + g(h-x\Psi) - hx\Omega\big],$$
$$\Gamma(\mathbf{x},\mathbf{y},\mathbf{d}) = \Omega^2[x^2+(l-y)^2] - 2gx\Omega + g^2 - (l-y)^2,$$

and abbreviated as Ξ, Υ and Γ. The only solution of (12) compatible with the AFO kinematics is as follows:

$$\alpha = \text{asin}\Big(\frac{-\Upsilon + \sqrt{\Upsilon^2 - 4\Xi\Gamma}}{2\Xi}\Big), \tag{13}$$

which is concluded from considering a known value of d, obtaining different values of the angle α from (13) and comparing them with the correct value of α which is obtained from the practical experiment.

After substituting the value of variables from Table I, the relationship between d and α becomes:

$$\alpha = \frac{\pi}{2} - \text{acos}\Big[-0.9 + \big(0.2 + 0.03\sqrt{-15.4 - \frac{93.4}{d^4} + \frac{164.3}{d^2}}\big)d^2\Big], \tag{14}$$

where d is in mm and α is in radians. This equation can be used to calculate the ankle angle from the linear potentiometer output.

IV. Dynamic Model of the Test-Bed

By treating the AFO-foot complex as a rigid body, its dynamics can be determined from the Euler-Lagrange equation:

$$\frac{\mathrm{d}}{\mathrm{d}t}(\frac{\partial\mathcal{L}}{\partial\dot{\alpha}}) - \frac{\partial\mathcal{L}}{\partial\alpha} = \Phi, \tag{15}$$

where Φ denotes the non-conservative generalized force, α denotes the ankle angle, and $\mathcal{L}$ is the Lagrange function, given by:

$$\mathcal{L} = E_\text{k} - E_\text{p}, \tag{16}$$

with E_k is the kinetic energy, and E_p is the potential energy. The kinetic energy can be expressed as:

$$E_\text{k} = \frac{1}{2}B(\alpha)\dot{\alpha}^2, \tag{17}$$

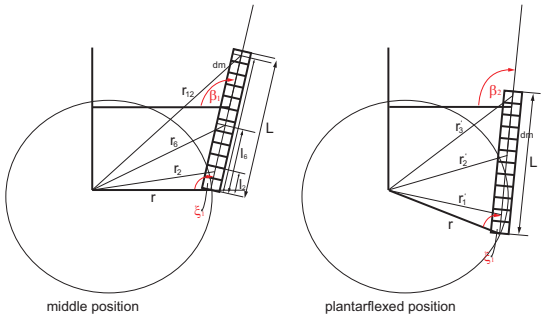

Fig. 3: The illustration of inertia of the motor's rod.

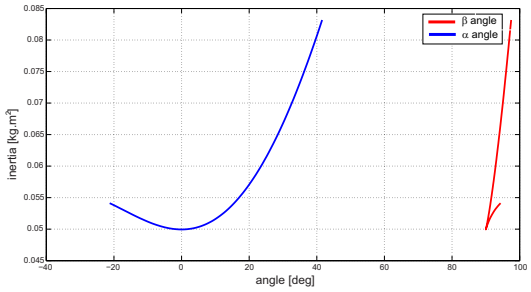

Fig. 4: The relation between angles α, β and the moment of inertia of motor's rod.

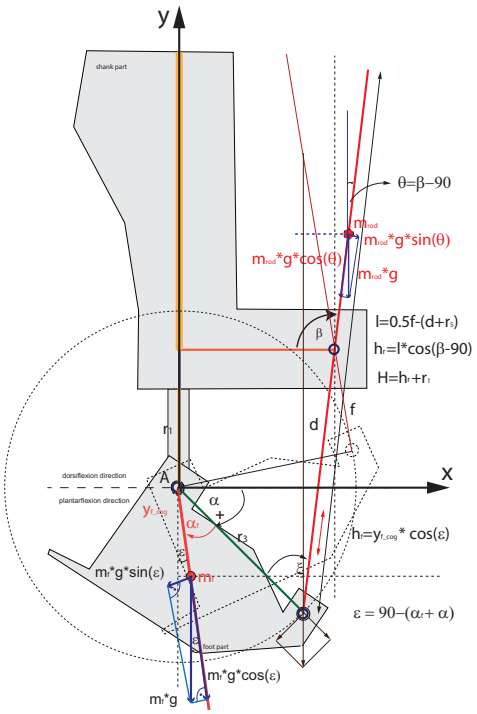

Fig. 5: The gravitation force of a foot, a collar and a rod.

where $B(\alpha) = I_{\mathrm{f}} + I_{\mathrm{c}} + I_{\mathrm{r}}(\alpha)$ denotes the comprehensive moment of inertia of the AFO's collar (I_{c}), the foot (I_{f}), and the motor's rod ($I_{\mathrm{r}}(\alpha)$).

It is worth mentioning that the inertia of the motor's rod depends on the ankle angle, as illustrated in Figure 3. Hence, the inertia changes due to the change of the movement angle ξ. The comprehensive inertia in a given position can be calculated by dividing the motor's rod into the infinitesimal elements and summing along the rod:

$$I_{\mathrm{r}}(\alpha) = \mathrm{d}m \sum_{i=1}^{N} r_i^2, \tag{18}$$

where $\mathrm{d}m$ is the mass of the infinitesimal element, N is the number of elements and r_i is the distance from the center position of each element and ankle rotation point that is given by:

$$r_i^2 = r^2 + l_i^2 - 2rl_i \cos\xi, \tag{19}$$

where r is the constant distance from the ankle rotation point to the point of motor's rod attachment, l_i is the corresponding distance from the attachment point of the motor's rod to the center of the i-th element, and ξ is the angle between vector r and the motor's rod. Figure 4 shows the change of $I_{\mathrm{r}}(\alpha)$ as a function of α and β. This relation can be used as a lookup table for modeling the AFO.

The moment of inertia of a foot and the AFO's collar are constant along the angular trajectory of α and were calculated numerically in a CAD application that modeled the AFO and foot. The resulted moment of inertias for the axis parallel to ankle joint's axis and passing through the central of mass are $I_{\mathrm{cy}} = 0.007\ \mathrm{kg.m^2}$ and $I_{\mathrm{fy}} = 0.022\ \mathrm{kg.m^2}$ for the AFO's collar and the foot, respectively, while their masses are $m_{\mathrm{cy}} = 0.151\ \mathrm{kg.m^2}$ and $m_{\mathrm{fy}} = 0.672\ \mathrm{kg}$ for the AFO's collar and the foot, respectively. The moment of inertia of the AFO's collar and the foot in relation to ankle were determined, using the Parallel Axis Theorem, to be:

$$I_{\mathrm{c}} = m_{\mathrm{cy}} d_{\mathrm{cy}}^2 + I_{\mathrm{cy}} = 0.151 \cdot 0.06^2 + 0.007 = 0.0075\mathrm{kg.m^2},$$
$$I_{\mathrm{f}} = m_{\mathrm{fy}} d_{\mathrm{fy}}^2 + I_{\mathrm{fy}} = 0.672 \cdot 0.08^2 + 0.022 = 0.0263\mathrm{kg.m^2}.$$

Moreover, the potential energy can be expressed as:

$$E_{\mathrm{p}} = E_{\mathrm{pf}} + E_{\mathrm{pA}}, \tag{20}$$

where E_{pf} is the potential energy of the foot, and E_{pA} that of the AFO.

Figure 5 shows the mass points and gravitation vectors, needed to define the potential energy. The potential energy E_{pf} is due to gravity only, as:

$$E_{\mathrm{pf}} = -m_{\mathrm{f}} g h_{\mathrm{f}} = -m_{\mathrm{f}} g y_{\mathrm{f}} \cos(\epsilon) = -m_{\mathrm{f}} g y_{\mathrm{f}} \sin(\alpha_{\mathrm{f}} + \alpha), \tag{21}$$

where y_{f} is the distance between foot's center of gravity to the ankle joint and is approximately equal to 0.08 m, $g = 9.8\ \mathrm{m/s^2}$ is gravitational acceleration, and α_{f} is a constant angle between the dorsal surface (upper part) of a foot and the middle of it. The potential energy of the AFO consists of:

$$E_{\mathrm{pA}} = E_{\mathrm{pc}} + E_{\mathrm{pr}}, \tag{22}$$

where E_{pc} and E_{pr} denote the potential energy of the AFO's collar and the motor's rod. The potential energy of the collar is, the analogy to the foot as follows:

$$E_{\text{pc}} = -m_{\text{c}} g y_{\text{c}} \sin(\alpha_{\text{f}} + \alpha),$$

where y_{c} is the distance between the collar's center of gravity and the ankle joint, and m_{c} is the collar mass. The potential energy of rod can be expressed as:

$$E_{\text{pr}} = m_{\text{rod}} g H = m_{\text{rod}} g (h_{\text{r}} + r_1) = m_{\text{rod}} g ((0.5f - d)\sin\beta + r_1),$$

and by substituting β from (10), it follows that:

$$E_{\text{pr}} = m_{\text{rod}} g ((0.5f - d)\sqrt{1 - \left(\Omega + \Psi \sin\alpha\right)^2} + r_1).$$

Differentiation of Lagrangian leads to:

$$\frac{\partial \mathcal{L}}{\mathrm{d}\alpha} = m_{\text{f}} g y_{\text{f}} \cos(\alpha_{\text{f}} + \alpha) + m_{\text{c}} g y_{\text{c}} \cos(\alpha_{\text{f}} + \alpha) - \frac{E_{\text{pr}}}{\mathrm{d}\alpha},$$
$$\frac{\partial \mathcal{L}}{\partial \dot{\alpha}} = (I_{\text{f}} + I_{\text{c}} + I_{\text{r}}(\alpha))\dot{\alpha}, \quad \frac{\mathrm{d}}{\mathrm{d}t}\left(\frac{\partial \mathcal{L}}{\partial \dot{\alpha}}\right) = (I_{\text{f}} + I_{\text{c}} + I_{\text{r}}(\alpha))\ddot{\alpha}.$$

It is very difficult to analytically differentiate rod's potential energy because there are many parameters which depend on α. However, the same result should be also obtained when applying Newton's laws to calculate the torque resulting from the rod as:

$$\frac{E_{\text{pr}}}{\mathrm{d}\alpha} = \tau_{\text{rod}} = -r_3 F_{\text{grav}} \sin(\xi) = -r_3 F_{\text{grav}} \sin(\beta - \alpha) = - r_3 m_{\text{rod}} g \cos(90 - \beta)\sin(\beta - \alpha) = - r_3 m_{\text{rod}} g \sin(\beta)\sin(\beta - \alpha). \quad (23)$$

The non-conservative force Φ includes all external forces/-torques and all forces/torques that depends on the path of travel and can be expressed as:

$$\Phi = r_3 k i \sin(\beta - \alpha), \quad (24)$$

where k is a torque constant of the motor, i is the motor's current. Therefore, the dynamic model of the ankle-foot complex + AFO is given as:

$$B(\alpha)\ddot{\alpha} + n(\alpha, \dot{\alpha}) = \tau, \quad (25)$$

where

$$B(\alpha) = (I_{\text{f}} + I_{\text{c}} + I_{\text{r}}(\alpha)), \quad \tau = i r_3 k \sin(\beta - \alpha),$$
$$n(\alpha, \dot{\alpha}) = -g(m_{\text{f}} y_{\text{f}} + m_{\text{c}} y_{\text{c}})\cos(\alpha_{\text{f}} + \alpha) - r_3 m_{\text{rod}} g \sin(\beta)\sin(\beta - \alpha). \quad (26)$$

V. Designated Torque Control

In order to prove that it is possible to control position and velocity of the AFO while commanding the torque, the *Designated Torque Control* framework (known also as the *Inverse Dynamics Control*) was tested. The designated torque control comes from the *Internal Model Principle*, which states that precise control can be achieved only if the control system encapsulates either implicitly or explicitly some representation

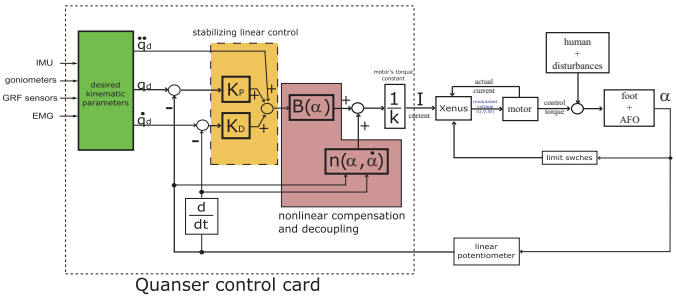

Fig. 6: The general structure of the designated torque controller in the context of the developed AFO.

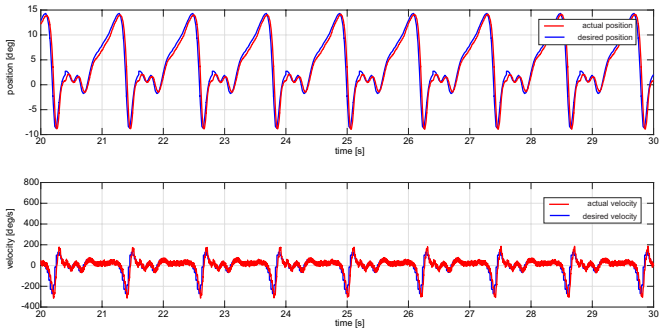

Fig. 7: Desired and actual position and velocity time history plots.

of the process to be controlled [16]. This control law is commonly used since after applying the nonlinear compensation and decoupling, the manipulator dynamics is replaced with a linear second-order subsystem.

By assuming that the control law can be expressed as:

$$\tau = B(\alpha)y + n(\alpha, \dot{\alpha}), \quad (27)$$

where y is a new input vector, then the classical choice for y is as follows:

$$y = \ddot{q}_{\text{d}} + K_{\text{P}}(q_{\text{d}} - \alpha) + K_{\text{d}}(\dot{q}_{\text{d}} - \dot{\alpha}), \quad (28)$$

where q_{d} is the desired angle of the ankle joint. Applying this control law to our system gave the control diagram in Figure 6.

This classical controller was modified; instead of using simple gains K_{p} and K_{d}, one gain was substituted by *PI* controller, where *I*-part was added because there was a steady-state error. The initial value of controller's gains were designated with the *Ziegler-Nichols* methods, and after that the parameters were improved during trial-and-error manual tuning.

To test this control framework the desired signal was used from the *OpenSim* Simulation [17] which was the time position of the right ankle joint during the normal walking. The experimental test by considering the designed controller was done and the results of the control can be viewed in Figure 7. It can be seen that despite of a simple control tuning method the robot was able to track the position and velocity of the

desired trajectory with a satisfactory accuracy. The accuracy of the position tracking was lower in the beginning of trajectory tracking due to wind-up effect (no wind-up filter was used), hence, tracking error could be further reduced by incorporating the anti-wind-up filter and by using more advanced controller e.g. by incorporating the feedforward part and by tuning the parameters of a controller for the variable inertia of the rod (LPV controller).

VI. Discussion

In this paper, the kinematic and dynamic equations of the combined system including the artificial leg and the AFO were obtained. It is worth mentioning that, these models provide valuable information about the system that might not be obtained in a purely experimental evaluation of the test-bed. Indeed, based on the system model, the designer can quickly evaluate the performance of system in a proper virtual environment, and can reduce the effort for both system hardware selection and control design. Moreover, the designer is able to address the critical issues in relation to the performance of the system before the device is used by a patient [8]. The developed model can be used to design and test different control strategies for the AFO before an experimental application.

It is worth mentioning that there exists some previous works in this field that derive the models for different types of AFOs [8], [13]–[15]. However, most of the considered AFOs are the rear-AFOs that are powered using SEA, hydraulic and pneumatic actuators. The considered AFO in this paper has a completely different structure than the previous mentioned AFOs. It is a front-AFO which is actuated using a ServoTube drive. Moreover, the actuator's forcer was not attached to the AFO's collar via its tip point which greatly increase the complexity of equations. Moreover, the considered AFO has a closed-loop chain structure which increase the difficulty of the system modelling.

An inverse dynamics control strategy was also proposed based on the AFO inverse dynamics. The proposed controller consists of two feedback loops, namely, an inner loop based on the AFO dynamic model, and an outer loop operating on the tracking error. The objective of the inner loop is to obtain a linear relationship for the system, whereas the outer loop is required to stabilize the overall system.

VII. Conclusion

In this paper, the kinematic and dynamic models of a new active AFO that characterized with a specific kinematic chain and a linear motor were derived. Then, the results from the real-time control experiment were presented. It was shown that using the proposed inverse dynamic controller the AFO is able to satisfactory track the desired position and velocity profiles. However, it should be mentioned that the designed controller is not robust to the existing disturbances in the system. Consequently, a robust sliding part can be added to the control structure to make the closed-loop system more robust with respect to existing uncertainties in the system. It should be noted that this is the first attempt in the literature which reports the results for the considered AFO.

References

[1] A. Gmerek, N. Meskin, E. S. Tehrani, and R. E. Kearney, "The characterization of the kinematic and dynamic properties of the ankle joint for an artificial ankle joint design," in *6th IEEE International Conference on Biomedical Robotics and Biomechatronics (BioRob)*, June 2016, pp. 710–716.

[2] C. Mavroidis, R. G. Ranky, M. L. Sivak, B. L. Patritti, J. DiPisa, A. Caddle, K. Gilhooly, L. Govoni, S. Sivak, M. Lancia, R. Drillio, and P. Bonato, "Patient specific ankle-foot orthoses using rapid prototyping," *Journal of NeuroEngineering and Rehabilitation*, vol. 8, no. 1, pp. 1–11, 2011.

[3] J. F. Geboers, M. R. Drost, F. Spaans, H. Kuipers, and H. A. Seelen, "Immediate and long-term effects of ankle-foot orthosis on muscle activity during walking: A randomized study of patients with unilateral foot drop," *Archives of Physical Medicine and Rehabilitation*, vol. 83, no. 2, pp. 240 – 245, 2002.

[4] R. Jimnez-Fabin and O. Verlinden, "Review of control algorithms for robotic ankle systems in lower-limb orthoses, prostheses, and exoskeletons," *Medical Engineering & Physics*, vol. 34, no. 4, pp. 397 – 408, 2012.

[5] Y. Bai, X. Gao, J. Zhao, F. Jin, F. Dai, and Y. Lv, "A portable ankle-foot rehabilitation orthosis powered by electric motor," *The Open Mechanical Engineering Journal*, vol. 9, no. 1, pp. 982–991, 2015.

[6] P. K. Jamwal, S. Hussain, and S. Q. Xie, "Review on design and control aspects of ankle rehabilitation robots," *Disabil Rehabil Assist Technol*, vol. 10, no. 2, pp. 93 – 101, 2015.

[7] J. A. Blaya and H. Herr, "Adaptive control of a variable-impedance ankle-foot orthosis to assist drop-foot gait," *IEEE Transactions on Neural Systems and Rehabilitation Engineering*, vol. 12, no. 1, pp. 24–31, March 2004.

[8] K. A. Shorter, Y. Li, T. Bretl, and E. T. Hsiao-Wecksler, "Modeling, control, and analysis of a robotic assist device," *Mechatronics*, vol. 22, no. 8, pp. 1067 – 1077, 2012.

[9] B. C. Neubauer, J. Nath, and W. K. Durfee, "Design of a portable hydraulic ankle-foot orthosis," in *36th Annual International Conference of the IEEE Engineering in Medicine and Biology Society*, Aug 2014, pp. 1182–1185.

[10] P. K. Jamwal, S. Q. Xie, S. Hussain, and J. G. Parsons, "An adaptive wearable parallel robot for the treatment of ankle injuries," *IEEE/ASME Transactions on Mechatronics*, vol. 19, no. 1, pp. 64–75, Feb 2014.

[11] A. Roy, H. I. Krebs, D. J. Williams, C. T. Bever, L. W. Forrester, R. M. Macko, and N. Hogan, "Robot-aided neurorehabilitation: A novel robot for ankle rehabilitation," *IEEE Transactions on Robotics*, vol. 25, no. 3, pp. 569–582, June 2009.

[12] A. M. Oymagil, J. K. Hitt, T. Sugar, and J. Fleeger, "Control of a regenerative braking powered ankle foot orthosis," in *IEEE 10th International Conference on Rehabilitation Robotics*, June 2007, pp. 28–34.

[13] Y. Bai, X. Gao, J. Zhao, F. Jin, F. Dai, and Y. Lv, "A portable ankle-foot rehabilitation orthosis powered by electric motor," *The Open Mechanical Engineering Journal*, vol. 9, pp. 982–991, 2015.

[14] Y.-L. Park, B. rong Chen, N. O. Prez-Arancibia, D. Young, L. Stirling, R. J. Wood, E. C. Goldfield, and R. Nagpal, "Design and control of a bio-inspired soft wearable robotic device for anklefoot rehabilitation," *Bioinspiration & Biomimetics*, vol. 9, no. 1, pp. 1–17, 2014.

[15] B. H. D.P. Ferris, J.M. Czerniecki, "An ankle-foot orthosis powered by artificial pneumatic muscles," *Journal of Applied Biomechanics*, vol. 21, pp. 189–197, 2005.

[16] B. Siciliano, L. Sciavicco, L. Villani, and G. Oriolo, *Robotics: Modelling, Planning and Control*, ser. Advanced Textbooks in Control and Signal Processing. Springer London, 2009.

[17] [Online]. Available: https://simtk.org/